Robotica (2022), **40**, pp. 762–779
doi:10.1017/S0263574721000795

CAMBRIDGE
UNIVERSITY PRESS

REPLY

Humanoid adaptive locomotion control through a bioinspired CPG-based controller

Chenpeng Yao[1,3], Chengju Liu[1,3,*], Li Xia[1], Ming Liu[2] and Qijun Chen[1]

[1]Department of Control Science and Engineering, Tongji University, Shanghai 201804, China, [2]Department of Electronic and Computer Engineering, the Hong Kong University of Science and Technology, Hong Kong 999077, China and [3]Tongji artificial intelligence (Suzhou) Research Institute, Suzhou 215000, China
*Corresponding author. Email: liuchengju@tongji.edu.cn

Received: 18 July 2020; **Revised:** 16 May 2021; **Accepted:** 17 May 2021; **First published online:** 22 June 2021

Keywords: Humanoid robot, Hierarchical central pattern generator (H-CPG), Adaptive locomotion, Workspace trajectory modulation, Bionic control

Abstract

To achieve adaptive gait planning of humanoid robots, a hierarchical central pattern generator (H-CPG) model with a basic rhythmic signal generation layer and a pattern formation layer is proposed to modulate the center of mass (CoM) and the online foot trajectory. The entrainment property of the CPG is exploited for adaptive walking in the absence of *a priori* knowledge of walking conditions, and the sensory feedback is applied to modulate the generated trajectories online to improve walking adaptability and stability. The developed control strategy is verified using a humanoid robot on sloped terrain and shows good performance.

1. Introduction

The bioinspired robotic control method draws nourishment from biological models or control mechanisms such as animal rhythmic motion generation, high-level control centers, and biological reflexes. In recent years, CPG-inspired control methods have attracted widespread attention in engineering and biologists. According to Grillner's definition [1], CPGs are referred to as a neural network that specializes in motion generation, and this network contains the necessary information to activate different motoneurons in proper sequence and strength to generate motion mode. These bioinspired control methods have been successfully applied to motion control of biomimetic robots [2, 3, 4]. Some well-known examples include a salamander robot [5], snake-shaped robot [6, 7], fish/dolphin-shaped robot [8, 9, 10], and multiped robot. [11, 12, 13, 14, 15, 16, 17] Meanwhile, the CPG mechanism has also been applied to the walking control of biped and humanoid robots [18, 19, 20, 21, 22, 23, 24].

Just like the entire control system of animal motion contains a complex feedback network, with the feedback mechanism, CPG-inspired control methods could have strong adaptability. Taga et al. [25] proposed the concept of global transmission to explain adaptive rhythmic motion. When a robot walks in a complex environment, it should make decisions based on environmental information such as topography and obstacles to determine the next step. Environmental information and robot status are merged in a high-level control center and then fed back to CPGs to control the output of the intelligent walking model. Therefore, to achieve an environmentally adaptive walk for a humanoid robot, the CPG feedback control model should be developed for different parts to receive feedback information. Currently, CPG engineering modeling adds feedback on top of the simplified biological neuron model and builds connections between neurons to generate multimodes. Fu et al. [26] achieved passive dynamics of walking with the hip joint driven by the parameterized oscillator, whose triggering and ceasing is modulated by feedback of the sensor. Fukuoka et al. [27] used CPG neuron with feedback from joint muscle's length and body

© The Author(s), 2021. Published by Cambridge University Press.

https://doi.org/10.1017/S0263574721000795 Published online by Cambridge University Press

inclination to realize the walking of a biped dinosaur-like robot. A deficiency of this modeling method is that sensing information is not easy to feed in, which makes it difficult to adapt. Moreover, feedback information only regulates the cycle and magnitude of the rhythmic locomotion and cannot provide a comprehensive and fast response to changes in the environment such as terrains, irregularities on the ground, and so on. Simple CPG neural network structure is not enough to model the complex motion of robot.

In order to model more complex CPG neural network structure of higher animals such as reptiles or mammals for walking motion, various CPG neural network structure models to explain such control mechanisms is developed. Brown [28] proposed one of the most classical structures named semi-center model structure. Klein et al. [29] designed a robotic leg, where the nerve structure, muscle, bone structure, and sensory feedback path in the human tissue system were simplified to simulate the human walking gait. Perret et al. [30] extended a conventional semi-center model and created a two-layer CPG control mechanism that controlled the motoneuron pulse time and action intensity. Burke et al. [31] introduced sensing information into an internuncial neuron layer and motoneuron layer to achieve hierarchical control of the motoneuron output based on the two-layer CPG neural network. Mcrea et al. [32] modified a conventional semi-center model and proposed a multilayer CPG neural network that accurately reflected the characteristics of biological rhythmic locomotion control.

With more accurate model, CPG-inspired control methods has been further developed and the corresponding feedback control models are created when different parts receive the feedback information, including the high-level control module, internuncial neuron, and motoneuron to solve the problem of voluntary walking in complex environments for the humanoid robot. Wang et al. [33] proposed a control strategy to simulate hierarchical biological CPG walking control and realized quadruped robot motion control. Auddy et al. [34] used an optimized CPG network for joint control and a neural network as the high-level controller to achieve bipedal locomotion in simulation. Endo et al. [35] adjusted the CPG control system parameters via a policy gradient-enhanced learning control method and achieved steady walking for a biped robot. Based on the nerve–muscle–bone system regulation mechanism, Fu et al. [36] investigated the bioinspired control of a biped robot with a system combining CPG and sensory feedback. Based on intensive learning and CPG/DMP, Santos et al. [37] investigated the humanoid robot walk in a sloped environment. Based on the vestibular reflex mechanism, in our previous work, we investigated the feedback information and the CPG control system integration strategy and effectively improved the walking capability of quadruped and biped robots [24, 38, 39]. The multilayer CPG structure somehow compensates the limitation of the single-layer CPG model and is a modeling method that is worthy of further investigation.

For a simple swimming or crawling robot, the CPG-based joint space control methods using one CPG unit to control one degree of freedom (DoF) of the robot are usually applied, so that the distributed oscillator network can generate complex coordinated multidimensional signals that are used as force or torque control to realize the coordinated motion. However, for a humanoid robot with more degree of freedom, many works continue to use such joint space control methods. Wang et al. [33] proposed a two-level CPG control mechanism to coordinate the drivers of robot joint, in which the output forces of joint drivers are controlled by the motoneurons with feedbacks in real time. Nassour et al. [40] used rhythm generator, pattern formation, and motoneuron (MN) layer to model one joint CPG controller that corresponds to one DC motor. Based on the multilayered multi-pattern CPG provided by Nassour[40], Tran et al. [41] used reinforcement learning to allow the robot to trigger a reaction to avoid falling. Mokhtari et al. [42] based on the CPG and ZMP achieve a hybrid adaptive robust control for a lower limb exoskeleton, where the CPG is applied to determine the desired angles of ankle, knee, and hip of both left and right legs. In our previous work [43], a ML-CPG was proposed and is used as the underlying low-level controller for a quadruped robot to generate adaptive walking patterns in joint place. Rhythm generation and pattern formation interneurons are modeled to promptly generate motion rhythm and patterns for motion sequence control, while motoneurons are modeled to control the output strength of the joint in real time according to feedback. For the reason that there are too many parameters to adjust, such joint space control methods cannot be applied effectively in humanoid walking.

https://doi.org/10.1017/S0263574721000795 Published online by Cambridge University Press

To overcome the limitations of conventional CPG control, a task space, or the so-called workspace-based humanoid robot walking control method using H-CPGs is proposed in this paper. Instead of the joint space method, the H-CPGs are used in the workspace of the humanoid to modulate the swinging phase and the supporting phase. Thus, the stance and swing phases are determined in real time by the output of the proposed multilayer CPG network to implement biped adaptive walking patterns. The presented method assigning H-CPGs to the periodic variables during robot locomotion simplifies the connections between CPGs and feedback pathways from the environment. Walking pattern adjustment of robots is easier to realize than the CPG joint space control method. This method can substantially reduce the number of CPGs and require less tuning of the parameters.

The main contributions are as follows:

1. A task space-based humanoid robot walking control method using H-CPGs is proposed.
2. Different to the common joint space control method that use each single CPG unit to control one degree of freedom (DoF) of the robot, the proposed method use CPG units to modulate the CoM and the foot trajectory of a humanoid robot to generate various adaptive walking patterns, so that it substantially reduce the number of CPGs and require less tuning of the parameters.
3. Adaptive biped walking in a sloped environments both in simulation and real robot are realized by integrating the robots posture feedback into foot trajectory generation in real time.

The remainder of the paper is organized as follows. Section 2 presents the model of the hierarchical CPG (H-CPG). Section 3 presents the control method of the H-CPG for the humanoid robot in the workspace. Simulations and experiments on the NAO robot are demonstrated in Section 4. Finally, some concluding remarks are offered in Section 5.

2. Hierarchical central pattern generator (H-CPG) model

As illustrated in Fig. 1, the entire control system consists of two major components: trajectory planning and a motion engine. The motion engine design includes kinematics and inverse kinematics, which aims to obtain a precise joint control signal based on the workspace trajectory. Trajectory planning includes CoM trajectory generation, workspace trajectory modulation, and feedback information input, the aim of which is to obtain adaptive walking trajectories with environmental information via H-CPGs. The proposed control method is general to legged robots. In this work, the humanoid NAO robot is used as an experiment platform and typical tests are designed to verify the proposed control method.

2.1. Architecture of the H-CPG

In this work, an H-CPG model is proposed. The novel model has a two-layer structure comprising of a basic rhythmic signal generation layer and a pattern formation layer. Unlike the common joint space control method, the CPG units are used in the workspace of the humanoid robot. That is, the proposed CPG model is used to modulate the CoM and the foot trajectory of a humanoid robot to generate various adaptive walking patterns. The basic H-CPG diagram for the proposed modulator, which is based on the control mechanism of neurophysiological studies, is shown in Fig. 2.

The proposed H-CPG architecture consists of two layers: rhythm generation neurons (RG) and pattern formation neurons (PF). In the rhythm generation layer, rhythmic signals are generated, and the associated parameters can be modulated easily. In the pattern formation layer, modulation signals of the movement patterns are generated to determine the different motion modes of modulated objects. The two layers can be regarded as an open structure with access ports in between and regulatory information implemented from the top. Because the sensory feedback modulates the movement of the hierarchical CPG neurons, the modulated object, environment, and CPG controller can constitute a closed-loop control system.

https://doi.org/10.1017/S0263574721000795 Published online by Cambridge University Press

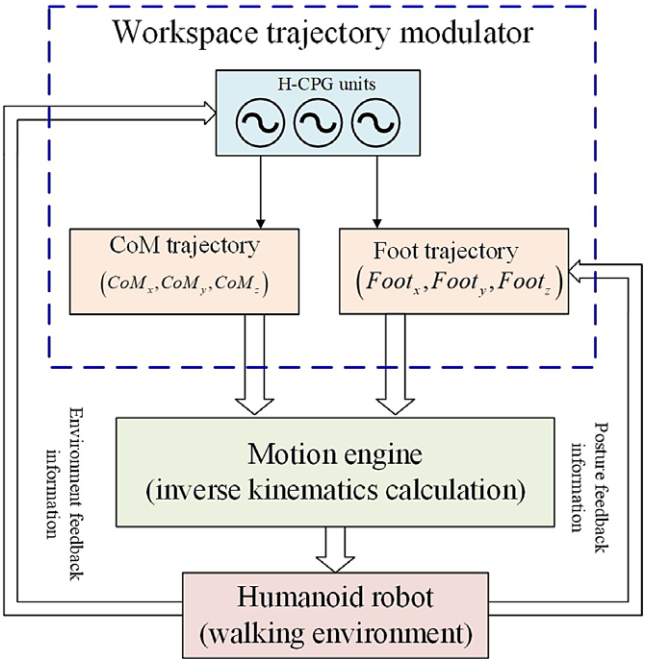


Figure 1. *Architecture of the biped walking control system.*

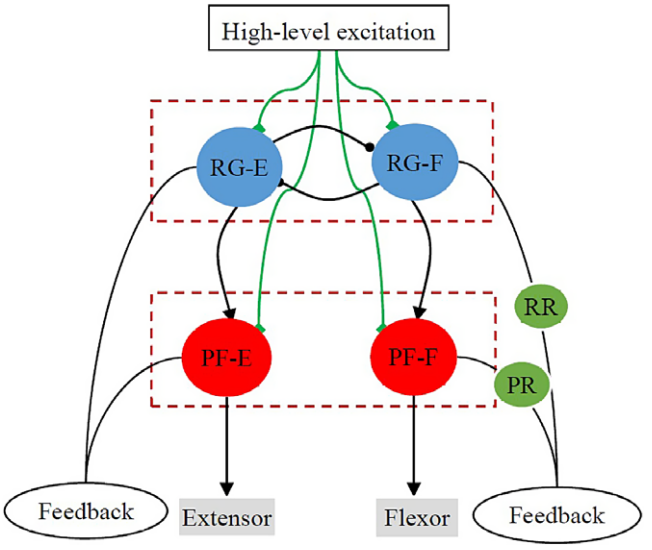


Figure 2. *Architecture of the proposed H-CPG. The rhythm reflection (RR) and pattern reflection (PR) represent the feedback of rhythm generation nerves and pattern formation nerves, respectively.*

2.2. Model of interneurons

Interneurons are required to rapidly respond to the environment and robot motion state and to control muscle motion sequences. The Hopfield continuous neuron model [24] is used to construct interneurons in this work. The generated mechanism of rhythms and patterns has the following characteristics: it does not have fixed rhythms and patterns, and it is motivated passively by external sensing information to determine the motion sequence of a robot. This neural model is parameterized using the following equation:

https://doi.org/10.1017/S0263574721000795 Published online by Cambridge University Press

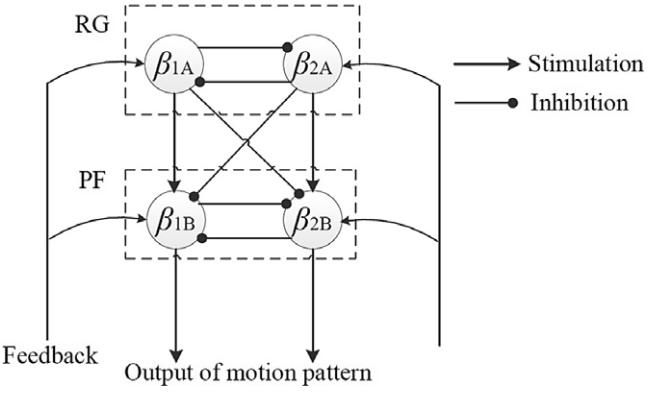


Figure 3. *Structure of the interneuron network.*

$$\begin{cases} \tau_i \frac{dy_i}{dt} = -\frac{y_i}{R_i} + \sum \omega_{ji}\sigma(x_j) \\ \sigma(x_j) = \left(1 + e^{(\Theta_j - x_j)}\right)^{-1} \end{cases} \tag{1}$$

where y_i represents the neuron membrane potential, τ_i is a time constant, and R_i is the damping coefficient of neuron conduction. x_j represents the jth feedback that a neuron receives. $\sigma(x_j)$ can be interpreted as the strength of external excitation on the neurons. ω_{ji} is the connection coefficient between neurons, while Θ_j is the role of the threshold of feedback x_j .

In a complex environment, robots must receive a variety of sensing information to generate the corresponding motion control signals. To ensure that the neuron model can quickly respond to feedback signals that exceed the neuron threshold value, the feedback item $\sum \omega_{ji}\sigma(x_j)$ in Eq. (1) is expended to $\sum_j T_{ji}g(y_i) + I_i$, where $\sum_j T_{ji}g(y_i)$ are feedbacks among neurons, while the $I_i \in [0, 1)$ is input items for external feedback information. For $\sum_j T_{ji}g(y_i)$, N is the number of neurons, and T_{ji} represents the connection coefficient between these neurons, $g(y)$ is an S-function expressed as $g\ (y) = \frac{1}{2}\ (1 + \tanh\ (2\sigma y))$. As for I_i, the interaction strength of the jth feedback is k_j, when the sensing information exceeds the threshold Θ_j, I_i rapidly grows and reaches its peak value. Furthermore, I_i stimulates the output of neurons to its peak value. In addition, y_i and u_i are the intermediate state and the final output of the neurons, respectively. In this model, a positive value of the intermediate state of a neuron y_i indicates that its drive muscle is active, while a zero value represents the corresponding muscle in a state of inhibition. A negative output of neurons has no practical significance in engineering; therefore, the final output item of a neuron is expressed as $u_i = \max\{y_i, 0\}$. Specially, the initial state is set as $y(t_0) = y^0 \in R^N$.

So that the Hopfield neural network is constructed by

$$\begin{cases} \tau_i \frac{dy_i}{dt} = -\frac{y_i}{R_i} + \sum_j T_{ji}g(y_i) + I_i, i = 1, \cdots, N \\ I_i = \left(1 + \sum_k e^{k_j(\Theta_j - x_j)}\right)^{-1} \\ u_i = \max\{y_i, 0\} \end{cases} \tag{2}$$

2.3. Stability analysis

As shown in Fig. 3, the neural network consists of a rhythm generator and a pattern generator, which are connected via stimulation and inhibition connections. The output of motion pattern are produced by receiving and processing the external sensing information.

https://doi.org/10.1017/S0263574721000795 Published online by Cambridge University Press

As an example, for $N = 4$, the dynamic model of the interneuron network is expressed as

$$\begin{cases} \tau_1 \frac{dy_1}{dt} = -\frac{y_1}{R_1} + T_{12} g_2(y_2) + I_1 \\ \tau_2 \frac{dy_2}{dt} = -\frac{y_2}{R_2} + T_{21} g_1(y_1) + I_2 \\ \tau_3 \frac{dy_3}{dt} = -\frac{y_3}{R_3} + T_{31} g_1(y_1) + T_{32} g_2(y_2) + T_{34} g_4(y_4) + I_3 \\ \tau_4 \frac{dy_4}{dt} = -\frac{y_4}{R_4} + T_{41} g_1(y_1) + T_{42} g_2(y_2) + T_{43} g_3(y_3) + I_4 \end{cases} \tag{3}$$

where each neuron is connected to another neuron of the same layer through inhibiting connections, while the different layers are connected through stimulating connections. The absolute values of the connection weights are set equal to each other, and the neural network connection matrix is set to

$$T_{ij} = \begin{vmatrix} 0 & -1 & 0 & 0 \\ -1 & 0 & 0 & 0 \\ 1 & -1 & 0 & -1 \\ -1 & 1 & -1 & 0 \end{vmatrix} \tag{4}$$

The stability of the neural network is analyzed, and the matrix W is set to

$$W = \frac{1}{2}\left(T_{ij} + T_{ij}^{\tau}\right) \tag{5}$$

According to Theorem 1 in ref. [38], we assume that the derivative of each activation function is positive and bounded. $\mu_{\max}$ is the maximum value of the eigenvalues of matrix W. For all $x \in R^1$, if $0 < g_i^{'}(x) \le \sigma_i$ and

$$\mu_{\max} < \frac{1}{\sigma_i R_i} \tag{6}$$

where $\sigma_i > 0,\ i = 1, \cdots, N$ and σ_i is the maximum value of $g_i^{'}(x)$, then the neural network in Eq. (3), the connection matrix of which is Eq. (4), has one and only one equilibrium point.

By calculating the eigenvalues of matrix W, $\mu_{\max} = 2$ is obtained. Then, when the range of parameters is satisfied, with $R_i\sigma_i < 0.5$, the neural network has only one equilibrium point. This condition applies to the parameter selection at the construction of the interneuron network to guarantee its stability. Letting the equilibrium state be $\bar{\mu}$ and $x_i = \mu_i - \bar{\mu}_i$, Eq. (3) becomes

$$\tau_i \frac{dx_i}{dt} = \sum_j T_{ij}\left(g_j(x_j + \bar{\mu}_j) - g_j(\bar{\mu}_j)\right) - \frac{x_i}{R_i},\ i = 1, 2, \cdots, 6 \tag{7}$$

Taking the Lyapunov function,

$$V(x) = \frac{1}{2}\sum_i \tau_i \alpha_i x_i^2 > 0 \tag{8}$$

and the derivative of Eq. (8) is

$$\begin{aligned} \frac{dV(x)}{dt} &= \sum_i \alpha_i x_i \left(\sum_j T_{ij}\left(g_j(x_j + \bar{\mu}_j) - g_j(\bar{\mu}_j)\right) - \frac{x_j}{R_i} \right) \\ &= \sum_i \alpha_i x_i \left(-\frac{x_j}{R_i} + \sum_j T_{ij}(g_j^{'}(\bar{\mu}_j)x_j + \frac{1}{2}g_j^{''}(\varepsilon_j)x_j^2) \right) \\ &= \le -\sum_i \frac{\alpha_i x_i^2}{R_i} + \sum_{ij} \alpha_i x_i T_{ij} \alpha_j x_j + \frac{1}{2}\alpha_i g^{''}(\varepsilon_j) \sum_{i=1}^{n} x_i^2 |x_i| \\ &= \le \sum_t \left(-\frac{1}{\sigma_i R_i} + \mu_{\max} + \frac{g^{''}(\varepsilon_j)}{2\sigma_i} \sum_{i=1}^{n} |x_i| \right) \sigma_i^2 x_i^2 \end{aligned} \tag{9}$$

https://doi.org/10.1017/S0263574721000795 Published online by Cambridge University Press

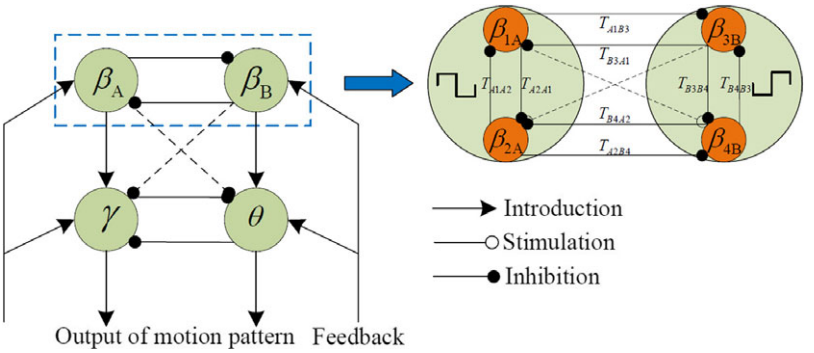


Figure 4. *Structure of the interneuron network for a humanoid.*

Suppose there are and that make the following formula valid:

$$-\frac{1}{\sigma_i R_i}+\mu_{\max}+\frac{g''(\varepsilon_j)}{2\sigma_i}\sum_{i=1}^{n}|x_i|<0 \tag{10}$$

We deduce from the theorem in ref. [38] that the equilibrium point of the above formula has exponential stability; that is, there are positive constants b_1, b_2 that make the following formula valid:

$$|\mu_i(t)-\bar{\mu}_i|=|x_i(t)|\le b_1\,|\mu_i(0)-\bar{\mu}_i|\,e^{[-b_2(t-t_0)]} \tag{11}$$

Because neurons are connected by inhibitory connections, $|y_i|<1$. Because the neural network of the two semi-central neurons inhibit each other, we have $\sum_{i=1}^{6}|y_i|<3$ and

$$g''(\varepsilon_j)=-4\sigma^2\tanh(2\sigma x)\mathrm{sech}^2(2\sigma x)<-2\sigma^2 \tag{12}$$

We can obtain

$$3\sigma_i+\frac{1}{\sigma_i R_i}>\mu_{\max} \tag{13}$$

Comparing $\mu_{\max}<\frac{1}{\sigma_i R_i}$ and Eq. (13), we conclude that when the system satisfies the condition that only one equilibrium point exists, the equilibrium must be exponentially stable.

3. H-CPG for humanoids

3.1. Structure of the interneuron network for humanoids

Considering bipedal walking, the robots left and right legs of A and B alternate on the ground to generate the walking movement. The proposed layered interneuron network is shown in Fig. 4. The circle represents a unit of the interneurons. The arrowed lines indicate introduction connections, and the rounded lines indicate inhibition of the connections. The symbol β represents rhythm generator neurons, A and B distinguish the left and right legs, respectively, and γ and θ represent the pattern generator neurons of leg A and leg B, respectively.

According to the connection of neurons and feedback, the basic motor rhythm is generated by the rhythm generator. Thus, the periodic rhythm signals of the left and right legs are generated according to the primary rhythmic feedback. To generate adaptive motion mode based on the rhythm output, the basic rhythm signals are inherited by the pattern generator. Then, the pattern generator can further generate the movement pattern according to the senior pattern feedback, and the adaptive modulation interface for the motion state is obtained.

https://doi.org/10.1017/S0263574721000795 Published online by Cambridge University Press

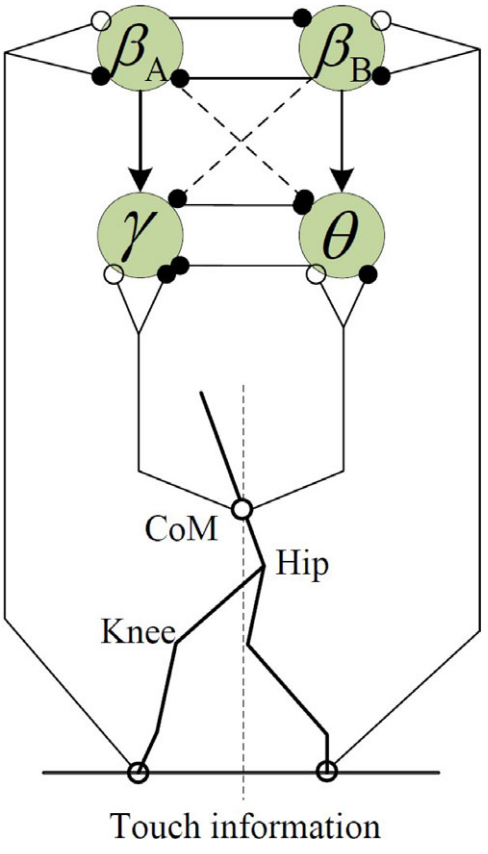


Figure 5. *Sensory feedback information.*

The internal connection of the two rhythm generators is shown in the right upper part of Fig. 4. The two groups of rhythmic CPG units (A and B) maintain phases opposite to each other through inhibiting and exciting connections. β_{1A}, β_{2A}, β_{3B}, and β_{4B} represent the four internal neurons of the rhythm generator and correspond to the extensor of leg A, the flexor of leg A, the extensor of leg B, and the flexor of leg B, respectively. The inhibitory connection between β_{1A} and β_{3B} maintains the opposite phases of leg A and leg B, and the excitation connections of β_{1A}, β_{3B} to β_{4B}, β_{2A} provide options to enhance the stability of the phase relationship. Finally, the combined output of the two neurons generates a rectangular wave of the opposite phase with respect to the feedback.

3.2. Feedback path of multi-sensor information

This subsection presents the construction of the feedback path of multiple sensor information in the control structure according to the study of the interaction state of the robot with its environment. The feedback path is shown in Fig. 5.

The sensory information introduced in the control system includes the robots own status information, such as the body inclination information and the foot contact information with environment. The body attitude information can reflect whether the robot is on a level surface or on a slope in real time. According to the body attitude state, the CoM of the robot can be adjusted, advanced, or retarded. The robots interaction status with the environment, such as plantar pressure information can reflect the contact state between the robot and the environment.

https://doi.org/10.1017/S0263574721000795 Published online by Cambridge University Press

3.3. Terrains interneuron network of the H-CPG

According to the biped robot rhythm generator connection structure, as shown in Fig. 4, the mathematical model of the rhythm generators of forelegs A and B is expressed as

$$\begin{cases} \tau_{\beta A1}\frac{dy_{\beta A1}}{dt} = -\frac{y_{\beta A1}}{R_{\beta A1}} + T_{A1A2}g_{\beta A2}\left(y_{\beta A2}\right) + T_{A1B3}g_{\beta B3}\left(y_{\beta B3}\right) + I_{\beta A1} \\ \tau_{\beta A2}\frac{dy_{\beta A2}}{dt} = -\frac{y_{\beta A2}}{R_{\beta A2}} + T_{A2A1}g_{\beta A1}\left(y_{\beta A1}\right) + T_{A2B4}g_{\beta B4}\left(y_{\beta B4}\right) \\ \qquad\qquad + T_{A2B3}g_{\beta B3}\left(y_{\beta B3}\right) + I_{\beta A2} \\ \tau_{\beta B3}\frac{dy_{\beta B3}}{dt} = -\frac{y_{\beta B3}}{R_{\beta B3}} + T_{B3B4}g_{\beta B3}\left(y_{\beta B3}\right) + T_{B3A1}g_{\beta A1}\left(y_{\beta A1}\right) + I_{\beta B1} \\ \tau_{\beta B4}\frac{dy_{\beta B4}}{dt} = -\frac{y_{\beta B4}}{R_{\beta B4}} + T_{B4B3}g_{\beta B4}\left(y_{\beta B4}\right) + T_{B4A1}g_{\beta A1}\left(y_{\beta A1}\right) \\ \qquad\qquad + T_{B4A2}g_{\beta A2}\left(y_{\beta A2}\right) + I_{\beta B2} \end{cases} \tag{14}$$

where the meanings of parameters τ, y , and so on are the same as in Eq. (2). The subscript β indicates that the layer of the neuron belongs to the rhythm generator, as shown in Fig. 4.

Second, the pattern generators of each leg are expanded, as shown in Fig. 4. Here, legs A and B are used in an example to build the mathematical model:

$$\begin{cases} \tau_{\gamma A}\frac{dy_{\gamma A}}{dt} = -\frac{y_{\gamma A}}{R_{\gamma A}} + T_{AeA1}g_{\beta A1}\left(y_{\beta A1}\right) + T_{AeA2}g_{\beta A2}\left(y_{\beta A2}\right) + I_{\gamma A} \\ \tau_{\theta A}\frac{dy_{\theta A}}{dt} = -\frac{y_{\theta A}}{R_{\theta A}} + T_{AfA2}g_{\beta A2}\left(y_{\beta A2}\right) + T_{AfA1}g_{\beta A1}\left(y_{\beta A1}\right) + I_{\theta A} \\ \tau_{\gamma B}\frac{dy_{\gamma B}}{dt} = -\frac{y_{\gamma B}}{R_{\gamma B}} + T_{BeB3}g_{\beta B3}\left(y_{\beta B3}\right) + T_{BeB4}g_{\beta B4}\left(y_{\beta B4}\right) + I_{\gamma B} \\ \tau_{\theta B}\frac{dy_{\theta B}}{dt} = -\frac{y_{\theta B}}{R_{\theta B}} + T_{BfB4}g_{\beta B4}\left(y_{\beta B4}\right) + T_{BfB3}g_{\beta B3}\left(y_{\beta B3}\right) + I_{\theta B} \end{cases} \tag{15}$$

where the meanings of parameters τ, y, etc., are the same as in Eq. (2). The subscripts γ and θ indicate that the layer of the neuron belongs to the pattern formation, and the subscripts e and f represent the extensor and flexor, respectively.

When walking in real environments, every layer of the H-CPG neural network must receive environmental feedback information. Therefore, it is necessary to add feedback items to each established neuron model. Here, leg A is used as an example to illustrate the sensing information and structure of each neuron. First, external feedback adjustment terms $I_{\beta A1}, I_{\beta A2}$ are added to the rhythm generator neurons β_{A1}, β_{A2}.

Figure 5 shows the rhythm generator, which chooses the movement phase after receiving information regarding contact between the feet and the ground. When the contact information is zero, the system determines that the robot is off the ground and switches to the swing phase. When the contact information exceeds a preset threshold, the system determines that the robot is in the phase of touchdown. The feedback terms $I_{\beta A1}, I_{\beta A2}$ are expressed as

$$\begin{cases} I_{\beta A1} = \left(1 + e^{k_{\beta A1}(\Theta_{c1} - x_c)}\right)^{-1} \\ I_{\beta A2} = \left(1 + e^{k_{\beta A2}(x_c - \Theta_{c2})}\right)^{-1} \end{cases} \tag{16}$$

where x_c is the value of the contact force between the foot and the ground, Θ_{ci} is the threshold of sensor information, and $k_{\beta i}$ is the interaction strength of the feedback. The meanings of the other parameters are the same as those in Eq. (1).

Then, external feedback adjustment terms $I_{\gamma A}, I_{\theta A}, I_{\gamma B}$, and $I_{\theta B}$ in the corresponding pattern generator neurons $\gamma_A, \theta_A, \gamma_B$, and θ_B are established. Figure. 5 shows the pattern generator, which chooses the movement behavior and sequence after receiving the body attitude information. When the robot is in a slope environment, the body produces a significant tilt angle, which breaks through the preset threshold of the pattern generator to further generate a new timing signal so that the system can

https://doi.org/10.1017/S0263574721000795 Published online by Cambridge University Press

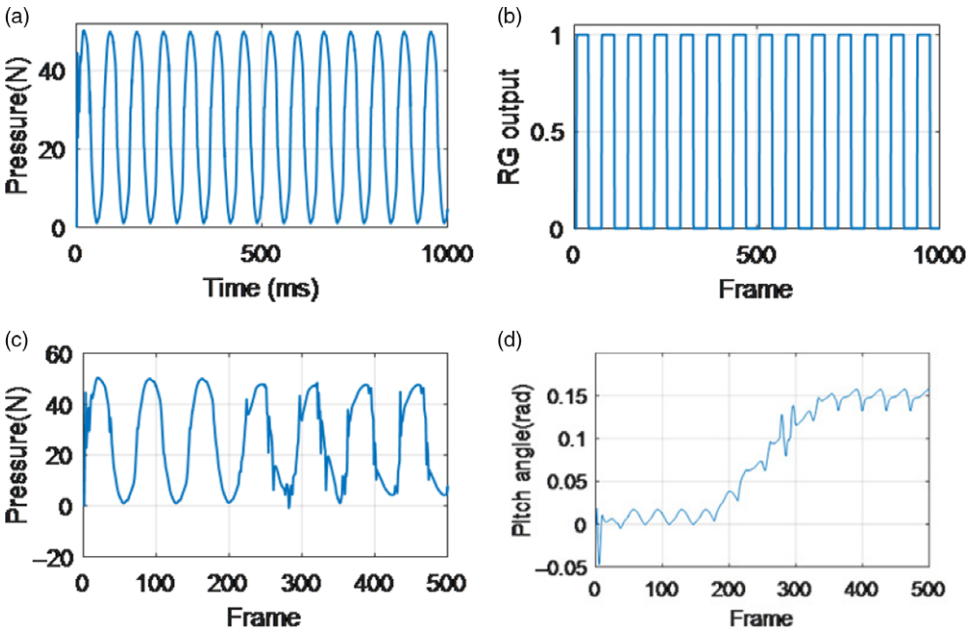


Figure 6. *The timing simulation of the H-CPG for biped walking.*

determine that the robot is on a slope and sends a modulation instruction. The feedback terms $I_{\gamma A}, I_{\theta A}$ are expressed as

$$\begin{cases} I_{\gamma A} = \left(1 + e^{k_{\gamma A}(\Theta_{\gamma A} - k_p \cdot |\theta_{pitch}|)}\right)^{-1} \\ I_{\theta A} = \left(1 + e^{k_{\theta A}(\Theta_{\theta A} - k_p \cdot |\theta_{pitch}|)}\right)^{-1} \end{cases} \tag{17}$$

where θ_{pitch} is the tilt angle of the robot body in the $x - z$ plane. The meanings of the other parameters are the same as those mentioned above. k_p is the intensity of the robot body angle sensing information. The feedback terms of $I_{\gamma B}, I_{\theta B}$ are similar to those of leg A.

3.4. The timing simulation of the H-CPG for biped walking

The core idea of the H-CPG model constructed for the workspace of the humanoid robot is to divide the motion sequence of legs using the state sensing information and evaluate the state of motion to adjust the CoM trajectory and the foot trajectory with the output signal.

First, in the rhythm layer, the rhythm generator receives pressure sensor information, generally periodic signals. Figure 6(a) shows the pressure value of the robot walking on the ground; the contact force is a sinusoid-like signal. Due to environmental disturbances and the jitter of the robots self-generated movement, the signal may contain aliasing signals such as sawtooth signals. In some cases, directly evaluating the movement state may cause severe errors.

Using the rhythm generator, the contact force information of the robot can be transformed into a standard periodic rectangular wave, which reflects the anti-interference ability of the neuron model. The output of the rhythm generator is shown in Fig. 6(b). An output of 1 indicates that leg A is in the supporting state, and an output of 0 indicates that leg A in the swinging state.

The pattern generation layer receives the body inclination information. Based on the periodic output of both feet in the rhythm layer, the pattern layer further outputs timings that indicate periodic swings of the two feet on the slope, which shows the sequence discrimination effect of the H-CPG. Figure 6(c) shows the plantar pressure curve of the robot from the ground to uphill for a process with significant

https://doi.org/10.1017/S0263574721000795 Published online by Cambridge University Press

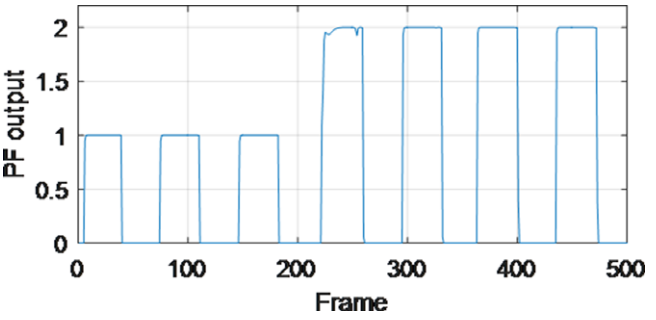


Figure 7. *Output of the pattern generator of the H-CPG from flat terrain to up slope terrain.*

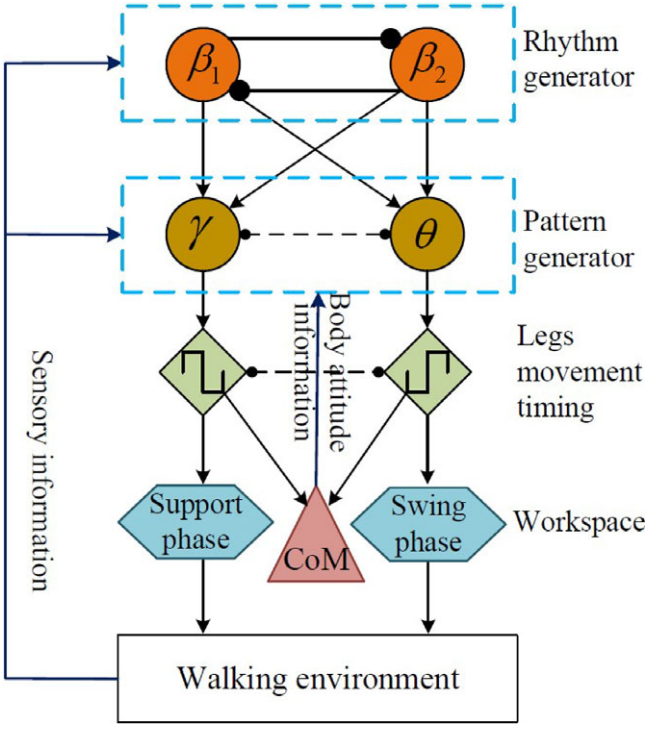


Figure 8. *Modulation mechanism of the workspace CPG-based method.*

disturbance. Figure 6(d) shows the curve of robot body inclination in the process from flat terrain to up-sloping terrain.

The output signal of the pattern generation layer under such a body attitude input is shown in Fig. 7. As can be observed, the multilayer CPG not only shows favorable anti-interference ability, but also converts the plantar pressure sawtooth waveform into a standard rectangular timing waveform to facilitate subsequent direct use of the signal. Furthermore, the rhythm generator and the pattern generator receive corresponding signals in sequence to address the effect of multi-sensor information, which not only maintains the output characteristics of the upper layer but also loads the lower layer information.

3.5. Workspace trajectory generator

The overall modulation mechanism structure is shown in Fig. 8. Using the state pattern of the leg movement timing output by the pattern generator, the advanced and delayed attitude of the CoM in

https://doi.org/10.1017/S0263574721000795 Published online by Cambridge University Press

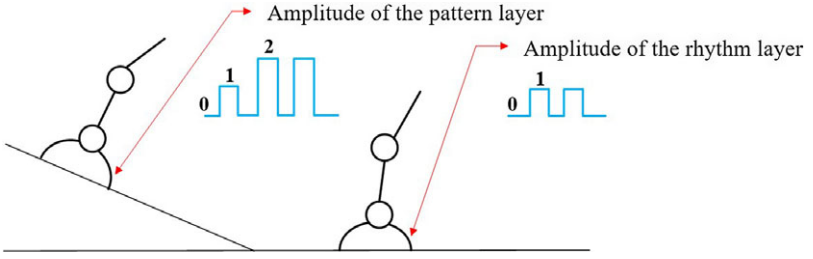


Figure 9. *Influence of a robots encounter with terrain on the CPG output.*

the workspace, the speed rhythm of the landing, and the landing are adjusted to realize the closed-loop adaptive interaction between the robot and the environment.

(1) CoM trajectory generation and modulation: A 3D linear inverted pendulum model (LIPM) is used to plan the CoM motion of the robot to generate a stable periodic gait. The position and velocity of the CoM, relative to the origin of the inverted pendulum, are given by

$$x(t) = x_0 \cosh(kt) + \dot{x}_0 \frac{1}{k} \sinh(kt) \tag{18}$$

$$\dot{x}(t) = x_0 k \sinh(kt) + \dot{x}_0 \cosh(kt) \tag{19}$$

where $k = \sqrt{g/h}$, g is the gravitational acceleration, h is the height of the CoM above the ground, and x_0 and $\dot{x}_0$ are the position and the velocity of the CoM relative to the origin of the inverted pendulum at $t = 0$, respectively.

Feedback loops are designed to make the CoM move forward along the slope and to reduce the step length during up-slope walking to maintain motion stability. In this work, the body attitude state θ_{pitch} is used as input sensory information to the trajectory generator to generate slope-adaptive trajectories.

Figure 9 shows that according to the presented feedback path, the robot adopts the output of its various layers as the standard timing modulated signal when crossing the terrain. Thus, using the output signals of the pattern formation layer, according to the state of the robot for an upward and downward slope, an online compensation strategy is designed as follows:

$$\mathrm{CoM}_{x_new} = \begin{cases} \begin{cases} \mathrm{CoM}_x + Feed, \theta_{pitch} > 0, & PF_u_\theta = 2 \\ \mathrm{CoM}_x - Feed, \theta_{pitch} < 0, & PF_u_\theta = 2 \end{cases} \\ \mathrm{CoM}_x, \qquad PF_u_\theta = 0 \end{cases} \tag{20}$$

Considering that the main change the robot detects during the uphill and downhill movement is the body attitude angle in the y direction and that the attitude angle in the x direction changes only minimally, the design strategy of the feedback via CoM trajectory is as follows:

$$Feed = K_{feed} \times \theta_{\mathrm{pitch_DC}}, \quad K_{\mathrm{feed}} > 0 \tag{21}$$

where K_{feed} is the feedback gain of the feedback term in the CPG model, and $\theta_{\mathrm{pitch_DC}}$ is the filtered body posture angle.

(2) Foot trajectory modulation: The output signal of the pattern generator is used to evaluate the walking terrain. If the terrain is uphill, the sensory feedback is used to adjust the interpolation ratio of the swing foot trajectory, thus generating adaptive movements that raise the feet slowly and settle quickly. When a downhill is detected to generate adaptive movements that raise feet quickly and settle slowly, the opposite strategy is used. The adjustment policy model is expressed as

$$\begin{cases} \eta = \begin{cases} 0.5 + K_\eta \cdot \theta_{pitch}, & PF_u_\gamma = 2 \\ 0.5, & PF_u_\gamma = 0 \end{cases} \\ up = \eta \cdot stepLen \end{cases} \tag{22}$$

https://doi.org/10.1017/S0263574721000795 Published online by Cambridge University Press

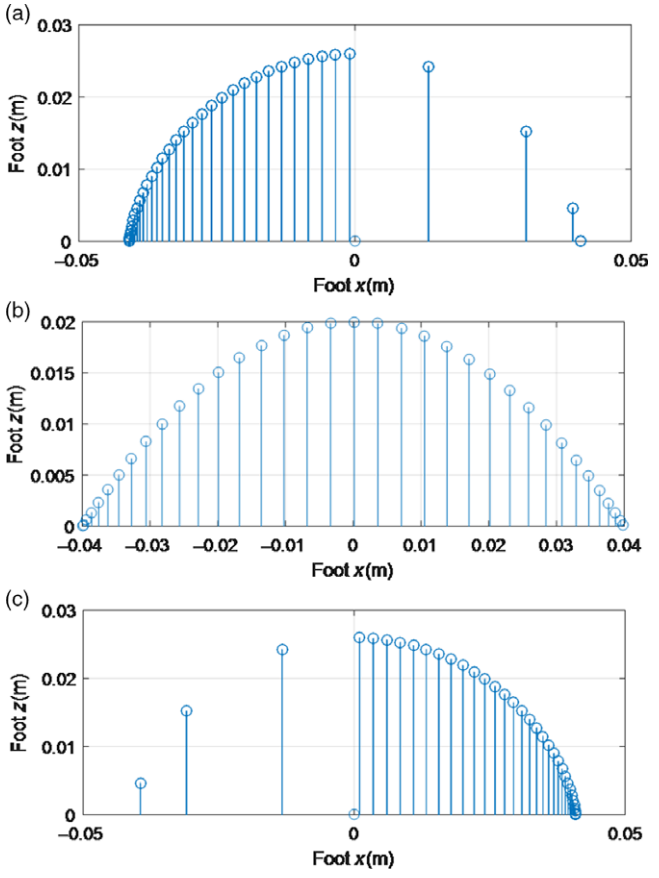


Figure 10. *Foot trajectory modulation. (a) Foot trajectory when walking uphill. (b) Foot trajectory when walking on flat terrain. (c) Foot trajectory when walking downhill.*

where *stepLen* is the overall frame of the foot trajectory and *up* is the frame of an upward foot. Using the body tilt θ_{pitch} to adjust the duty cycle η and to ensure the generation of a reasonable allocation of frames of the upward and downward feet, the adjustable can be expressed as

$$\theta = \begin{cases} step \cdot \pi / up, & step <= up \\ \pi + (step - up) \cdot \pi / (stepLen - up), & step > up \end{cases} \tag{23}$$

where *step* is the interval per frame. According to the distribution of the number of points to determine the rolling angle of each frame, to generate the speed of the foot lift, the cycloid trajectory is expressed as

$$\begin{cases} P_x = a(\theta - \sin(\theta)) \\ P_z = a(1 - \cos(\theta)) \end{cases} \tag{24}$$

According to the cycloid equation, Fig. 10 shows the selected simulation examples of foot trajectories when walking uphill, on flat terrain, and downhill, when going up the slope, the foot raises slowly and falls quickly, while when going down the slope, the foot raises quickly and falls slowly, and in the middle, the foot passes smoothly, which shows a good adaptability to the environment, and demonstrates the effectiveness of frame modulation according to feedback information.

https://doi.org/10.1017/S0263574721000795 Published online by Cambridge University Press

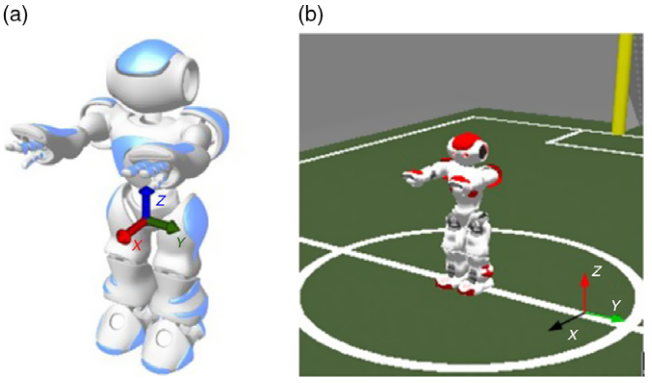


Figure 11. *The robot platform. (a) NAO robot. (b) ODE-based simulation environment.*

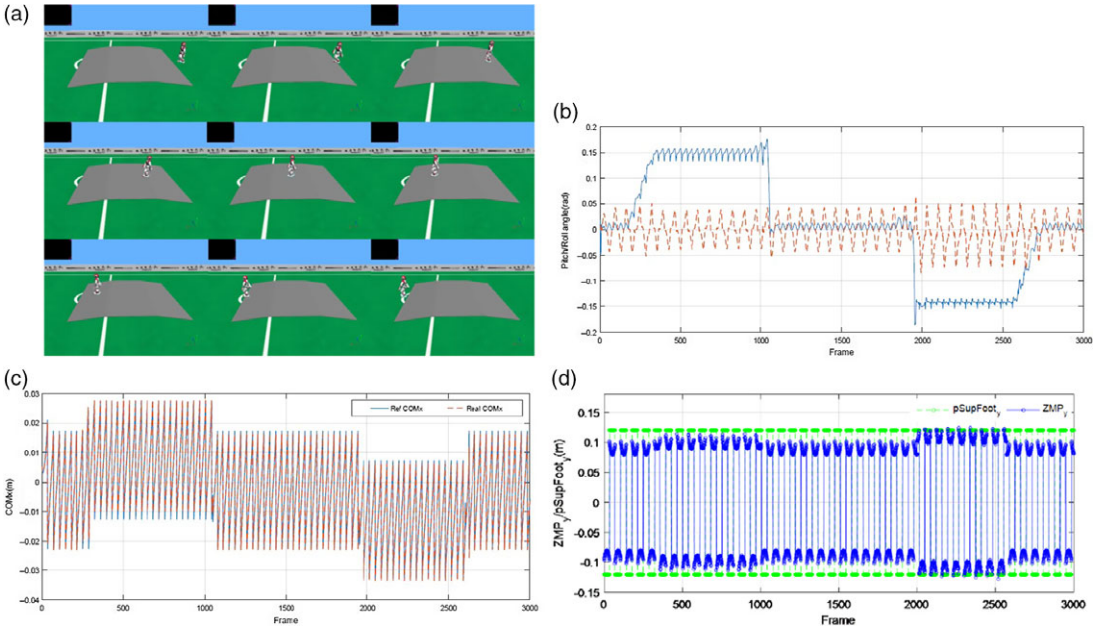


Figure 12. *Simulation experiment results of walking up and down a slope with body attitude feedback. (a) Side view screenshots of the simulation experiment. (b) Body attitude during sloped terrain walking. (c) Modulated CoM trajectory during sloped terrain walking. (d) ZMP distribution in the y direction during sloped terrain walking.*

4. Simulations and experiments

Simulations and real robot experiments are setup using the humanoid NAO platform (Fig. 11(a)). NAO has 26 degrees of freedom. Simulations are conducted using the Webots simulation platform as shown in Fig. 11(b).

4.1. Experiment on a simulated humanoid robot

A slope (10 degree) adaptive walking simulation experiment was conducted for 56 s. The gait pattern can be adjusted autonomously to realize uphill and downhill walking. Figure 12(a) shows side view

https://doi.org/10.1017/S0263574721000795 Published online by Cambridge University Press

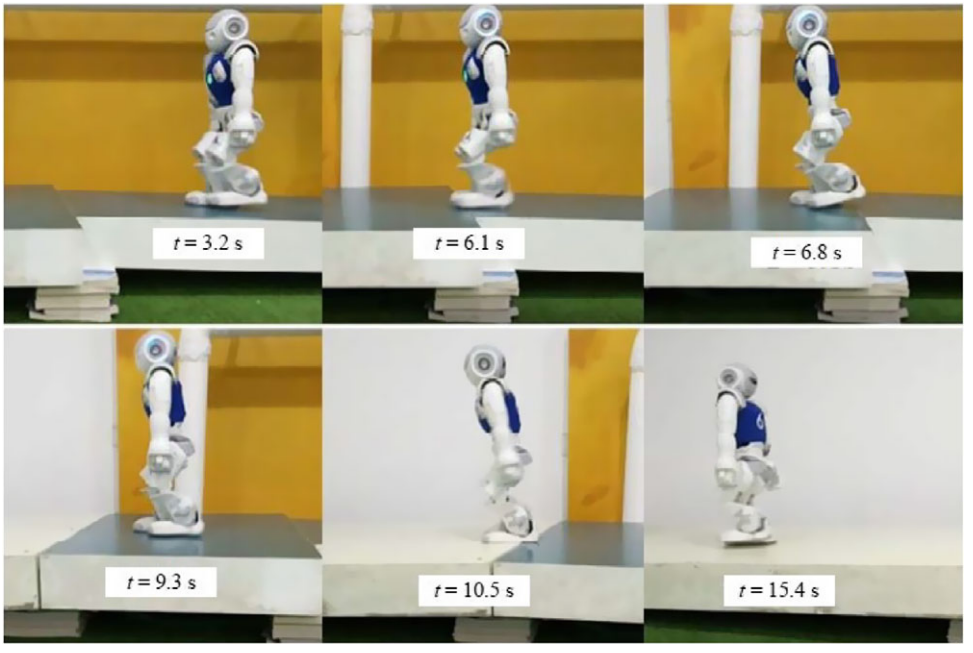


Figure 13. *Side view screenshots of the simulation experiment.*

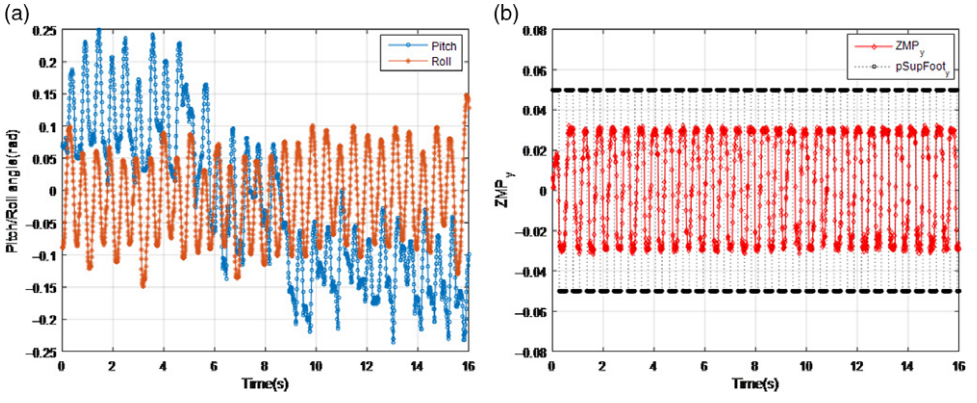


Figure 14. *The experimental data of the robot corresponding to Fig. 13. (a) The body posture angle of NAO robot. (b) ZMP of NAO in y direction.*

screenshots of the simulation experiment. Figure 12(b) shows θ_{pitch}, which represents the changes of the body attitude of NAO. As shown in Fig. 12(c), coupled with the θ_{pitch}, the position of CoMx and the walking patterns with adaptive step length can be adaptively modulated. Figure 12(d) shows the distribution of the ZMP during sloped terrain walking. The whole slope adaptive walking simulation experiment experienced five stages: flat, uphill, flat, downhill, and flat. In the uphill process (about frame 300 to frame 1000), the body attitude of the robot (Fig. 12(b)) becomes larger when compared to the flat stage (about frame 0 to frame 300), our controller adjusts the CoM trajectory (Fig. 12(c)) according to the feedback and make it more forward to keep the robot in balance. Accordingly, this change also affects the ZMP trajectory (Fig. 12(d)), trying to make a larger step. On the contrary, the θ_{pitch} decreased in the downhill process (about frame 1900 to frame 2000), so that our controller try to set the CoM more backward to avoid falling. With the effect of the proposed controller, the NAO robot is able to maintain stability and satisfactory stability margins.

https://doi.org/10.1017/S0263574721000795 Published online by Cambridge University Press

4.2. Real robot experiment

One experiment was conducted to test the robots performance without prior knowledge of the walking terrain. The experiment allowed the robot to walk over three stages of an inclined terrain (approximately slopes with 6°), and the connected stage consisted of flat terrain. The walking surface was an elastically deformable platform, and the friction coefficient between the feet and the walking surface was not large enough to avoid slippage. Every step of NAO on the platform could cause the walking surface to deform, and slippage could occur. During the inclined terrain walking, the body attitude-based feedback paths were used to adjust the generated CoM and foot trajectories automatically. The experiment snapshots are shown in Fig. 13 and the corresponding datas of Fig. 13 are shown in Fig. 14.

The differences between Webots simulations and real experiments are due to the measurement noise, offset, and robot model uncertainties, including joint compliance and the slip between the feet of the NAO and the walking surface. The NAO robot showed only a small amount of staggering during the terrain transitions. The experiments show that the generated trajectories are applicable and workable.

5. Conclusions

A novel H-CPG model was developed and applied in the adaptive locomotion control of humanoid robots in this work. The proposed CPG model was used to modulate the CoM and the online foot trajectory of a humanoid robot to generate various adaptive gait patterns. Using a motion engine, the characteristics of the workspace were mapped to the joint space. Sensory feedback was exploited to modulate the generated trajectories in real time for adaptive walking in the absence of *a priori* knowledge of walking conditions. The developed control strategy was verified using a humanoid robot on sloped terrains. This work employs the dynamic properties of the presented H-CPG model to develop an online trajectory generation method. In this method, the H-CPG in the workspace was allocated to generate trajectories for the robot to simplify the design of the connection weights and feedback pathways. Moreover, by entraining feedback loops to prevent slippage and overturning, the robot can negotiate steeper slopes than the conventional control method.

The proposed walking control strategy effectively uses a CPG-inspired workspace trajectory modulator for biped robots to overcome the limitations of the conventional trajectory-based control methods and the CPG-inspired joint space control methods. This paper demonstrates the potential of the CPG concept in the study of dynamic walking of biped robots. To achieve adaptability in complex environments, blind walking is infeasible. In future work, topographical information for robot walking, for example, obstacles, gradient, and surface roughness, should be described in detail. Vision and other sensing information should be leveraged to sense the environment and integrate the environmental information to improve the walking capability.

Acknowledgment. This work was supported in part by the National Natural Science Foundation of China (U1713211, 61733013, 61673300) and Jiangsu Key Research and Developement Project (BE2020101).

Supplementary Material. To view supplementary material for this article, please visit https://doi.org/10.1017/S0263574721000795.

References

[1] S. Grillner, "Biological pattern generation: The cellular and computational logic of networks in motion," *Neuron.* **52**(5), 751–766 (2006).

[2] A. J. Ijspeert, "Central pattern generators for locomotion control in animals and robots: A review," *Neural Networks* **21**(4), 642–653 (2008).

[3] Q. Wu, C. Liu, J. Zhang and Q. Chen, "Survey of locomotion control of legged robots inspired by biological concept," *Sci. Ser. F Inf. Sci.* **52**(10), 1715–1729 (2009).

https://doi.org/10.1017/S0263574721000795 Published online by Cambridge University Press

[4] J. Yu, M. Tan, J. Chen and J. Zhang, "A survey on CPG-inspired control models and system implementation," *IEEE Trans. Neural Networks Learn. Syst.* **25**(3), 441–456 (2013).
[5] D. Ryczko, J. Knüsel, A. Crespi, S. Lamarque, A. Mathou, A. J. Ijspeert and J.-M. Cabelguen, "Flexibility of the axial central pattern generator network for locomotion in the salamander," *J. Neurophysiol.* **113**(6), 1921–1940 (2015).
[6] Z. Wang, Q. Gao and H. Zhao, "CPG-inspired locomotion control for a snake robot basing on nonlinear oscillators," *J. Intell. Rob. Syst.* **85**(2), 209–227 (2017).
[7] X. Wu and S. Ma, "Neurally controlled steering for collision-free behavior of a snake robot," *IEEE Trans. Control Syst. Technol.* **21**(6), 2443–2449 (2013).
[8] J. Yu, Z. Wu, M. Wang and M. Tan, "CPG network optimization for a biomimetic robotic fish via PSO," *IEEE Trans. Neural Networks Learn. Syst.* **27**(9), 1962–1968 (2015).
[9] J. Yu, C. Wang and G. Xie, "Coordination of multiple robotic fish with applications to underwater robot competition," *IEEE Trans. Ind. Electr.* **63**(2), 1280–1288 (2015).
[10] T. Wang, Y. Hu and J. Liang, "Learning to swim: A dynamical systems approach to mimicking fish swimming with CPG," *Robotica* **31**(3), 361 (2013).
[11] X. Zhang, J. Gong and Y. Yao, "Effects of head and tail as swinging appendages on the dynamic walking performance of a quadruped robot," *Robotica* **34**(12), 2878–2891 (2016).
[12] G. Zhong, L. Chen, Z. Jiao, J. Li and H. Deng, "Locomotion control and gait planning of a novel hexapod robot using biomimetic neurons," *IEEE Trans. Control Syst. Technol.* **26**(2), 624–636 (2017).
[13] T. Fukui, H. Fujisawa, K. Otaka and Y. Fukuoka, "Autonomous gait transition and galloping over unperceived obstacles of a quadruped robot with CPG modulated by vestibular feedback," *Rob. Auto. Syst.* **111**, 1–19 (2019).
[14] Z. Ma, Y. Liang and H. Tian, "Research on Gait Planning Algorithm of Quadruped Robot Based on Central Pattern Generator," *2020 39th Chinese Control Conference (CCC)* (2020) pp. 3948–3953.
[15] X. Wang, H. Liu, B. Liang, X. Wang and J. Yang, "Locomotion Control for Quadruped Robot Combining Central Pattern Generators with Virtual Model Control," *2019 IEEE 15th International Conference on Control and Automation (ICCA)* (2019) pp. 399–404.
[16] D. Zhang, J. Wu, Q. Zhu, R. Xiong, Y. Zhang, Y. Zhu and J. Xu, "A Fuzzy Control Method Based on Central Pattern Generator for Quadrupedrobots," *2019 Chinese Automation Congress (CAC)* (2019) pp. 861–866.
[17] A. S. Lele, Y. Fang, J. Ting and A. Raychowdhury, "Learning to walk: Bio-mimetic hexapod locomotion via reinforcement based spiking central pattern generation," *IEEE J. Emerging Sel. Top. Circ. Syst.* **10**(4), 1–1 (2020).
[18] W. Huang, C.-M. Chew and G.-S. Hong, "A coordination-based CPG structure for 3d walking control," *Robotica* **31**(5), 777 (2013).
[19] A. A. Saputra, J. Botzheim, I. A. Sulistijono and N. Kubota, "Biologically inspired control system for 3-d locomotion of a humanoid biped robot," *IEEE Trans. Syst. Man Cybern. Syst.* **46**(7), 898–911 (2015).
[20] A. Shachykov, O. Shuliak and P. Hnaff, "Closed-Loop Central Pattern Generator Control of Human Gaits in Opensim Simulator," *2019 International Joint Conference on Neural Networks (IJCNN)* (2019) pp. 1–8.
[21] Y.-D. Hong, C.-S. Park and J.-H. Kim, "Stable bipedal walking with a vertical center-of-mass motion by an evolutionary optimized central pattern generator," *IEEE Trans. Ind. Electr.* **61**(5), 2346–2355 (2013).
[22] C.-F. Juang and Y.-T. Yeh, "Multiobjective evolution of biped robot gaits using advanced continuous ant-colony optimized recurrent neural networks," *IEEE Trans. Cybern.* **48**(6), 1910–1922 (2017).
[23] Y. Wang, X. Xue and B. Chen, "Matsuoka's CPG with desired rhythmic signals for adaptive walking of humanoid robots," *IEEE Trans. Cybern.* **50**(2), 613–626 (2018).
[24] C. Liu, D. Wang, E. D. Goodman and Q. Chen, "Adaptive walking control of biped robots using online trajectory generation method based on neural oscillators," *J. Bionic Eng.* **13**(4), 572–584 (2016).
[25] G. Taga, Y. Yamaguchi and H. Shimizu, "Self-organized control of bipedal locomotion by neural oscillators in unpredictable environment," *Biol. Cybern.* **65**(3), 147–159 (1991).
[26] C. Fu, F. Tan and K. Chen, "A simple walking strategy for biped walking based on an intermittent sinusoidal oscillator," *Robotica* **28**(6), 869 (2010).
[27] Y. Fukuoka and J. Akama, "Dynamic bipedal walking of a dinosaur-like robot with an extant vertebrate's nervous system," *Robotica* **32**(6), 851 (2014).
[28] T. G. Brown, "On the nature of the fundamental activity of the nervous centres; together with an analysis of the conditioning of rhythmic activity in progression, and a theory of the evolution of function in the nervous system," *J. Physiol.* **48**(1), 18 (1914).
[29] T. J. Klein and M. A. Lewis, "A physical model of sensorimotor interactions during locomotion," *J. Neural Eng.* **9**(4), 046011 (2012).
[30] C. Perret, J.-M. Cabelguen and D. Orsal, "Analysis of the Pattern of Activity in "Knee Flexor" Motoneurons During Locomotion in the Cat," **In:** *Stance and Motion* (Springer, 1988) pp. 133–141.
[31] R. Burke, A. Degtyarenko and E. Simon, "Patterns of locomotor drive to motoneurons and last-order interneurons: Clues to the structure of the CPG," *J. Neurophysiol.* **86**(1), 447–462 (2001).
[32] D. A. McCrea and I. A. Rybak, "Organization of mammalian locomotor rhythm and pattern generation," *Brain Res. Rev.* **57**(1), 134–146 (2008).

https://doi.org/10.1017/S0263574721000795 Published online by Cambridge University Press

[33] T. Wang, W. Guo, M. Li, F. Zha and L. Sun, "CPG control for biped hopping robot in unpredictable environment," *J. Bionic Eng.* **9**(1), 29–38 (2012).
[34] S. Auddy, S. Magg and S. Wermter, "Hierarchical Control for Bipedal Locomotion Using Central Pattern Generators and Neural Networks," *2019 Joint IEEE 9th International Conference on Development and Learning and Epigenetic Robotics (ICDL-EpiRob)* (2019) pp. 13–18.
[35] G. Endo, J. Morimoto, T. Matsubara, J. Nakanishi and G. Cheng, "Learning CPG-based biped locomotion with a policy gradient method: Application to a humanoid robot," *Int. J. Rob. Res.* **27**(2), 213–228 (2008).
[36] C. Fu, J. Wang, K. Chen, Z. Yu and Q. Huang, "A walking control strategy combining global sensory reflex and leg synchronization," *Robotica* **34**(5), 973 (2016).
[37] J. André, C. Teixeira, C. P. Santos and L. Costa, "Adapting biped locomotion to sloped environments," *J. Intell. Rob. Syst.* **80**(3–4), 625–640 (2015).
[38] C. Liu, Q. Chen and D. Wang, "CPG-inspired workspace trajectory generation and adaptive locomotion control for quadruped robots," *IEEE Trans. Syst. Man Cybern. Part B (Cybern.)* **41**(3), 867–880 (2011).
[39] C. Liu, D. Wang and Q. Chen, "Central pattern generator inspired control for adaptive walking of biped robots," *IEEE Trans. Syst. Man Cybern. Syst.* **43**(5), 1206–1215 (2013).
[40] J. Nassour, P. Hénaff, F. Benouezdou and G. Cheng, "Multi-layered multi-pattern CPG for adaptive locomotion of humanoid robots," *Biol. Cybern.* **108**(3), 291–303 (2014).
[41] D. H. Tran, F. Hamker and J. Nassour, "A humanoid robot learns to recover perturbation during swinging motion," *IEEE Trans. Syst. Man Cybern. Syst.* **50**(10), 3701–3712 (2018).
[42] M. Mokhtari, M. Taghizadeh and M. Mazare, "Hybrid adaptive robust control based on CPG and ZMP for a lower limb exoskeleton," *Robotica* **39**(2), 181–199 (2021).
[43] C. Liu, L. Xia, C. Zhang and Q. Chen, "Multi-layered CPG for adaptive walking of quadruped robots," *J. Bionic Eng.* **15**(2), 341–355 (2018).

Cite this article: C. Yao, C. Liu, L. Xia, M. Liu and Q. Chen (2022). "Humanoid adaptive locomotion control through a bioinspired CPG-based controller", Robotica **40**, 762–779. https://doi.org/10.1017/S0263574721000795

https://doi.org/10.1017/S0263574721000795 Published online by Cambridge University Press